REPORT DOCUMENTATION PAGE

Form Approved
OMB No. 0704-0188

1. REPORT DATE *(DD-MM-YYYY)*	2. REPORT TYPE	3. DATES COVERED *(From - To)*
11/10/2011	Final Performance Report	08/15/2009-08/14/2011

4. TITLE AND SUBTITLE

Non-Born-Oppenheimer Spectroscopy of Cyclic Triatomics

5a. CONTRACT NUMBER

5b. GRANT NUMBER
FA9550-09-1-0604

5c. PROGRAM ELEMENT NUMBER

6. AUTHOR(S)

Dmitri A. Babikov, Ph.D.

5d. PROJECT NUMBER

5e. TASK NUMBER

5f. WORK UNIT NUMBER

7. PERFORMING ORGANIZATION NAME(S) AND ADDRESS(ES)

Marquette University
Office of the Comptroller
915 W. Wisconsin Avenue, Room 175,
Milwaukee, WI 53233-2310

8. PERFORMING ORGANIZATION REPORT NUMBER

9. SPONSORING / MONITORING AGENCY NAME(S) AND ADDRESS(ES)

Air Force Office of Scientific Research
Attn: Mary Moore-PKC
875 North Randolph Street
Suite 325, Rm. 3122
Arlington, Virginia 22203-1768

10. SPONSOR/MONITOR'S ACRONYM(S)

11. SPONSOR/MONITOR'S REPORT NUMBER(S)
AFRL-OSR-VA-TR-2012-0732

12. DISTRIBUTION / AVAILABILITY STATEMENT

For Public Release

13. SUPPLEMENTARY NOTES

14. ABSTRACT

This project involved theoretical and computational studies of quantum dynamics and spectroscopy in the presence of conical intersection, where the Born-Oppenheimer approximation fails due to a very significant geometric phase effect. The focus was on cyclic-N_{3}. Spectroscopy of this radical was studied in great detail, which included construction of its potential energy surface and dipole moment function in the entire configuration space around the conical intersection, accurate calculations of its vibrational states using the state-of-the-art approach (gauge theory), detailed analysis of the geometric phase effect, calculation of transition intensities and, finally, prediction of its infrared spectrum. A simplified treatment of the pseudo-rotational spectrum has also been proposed, based on perturbation theory, which should help to analyze experimental spectrum of cyclic-N_{3} (when it becomes available) and identify this mysterious molecule in the lab. It should also allow deriving major properties of potential energy surface of cyclic-N_{3} directly from the experimental data. In addition, new global potential energy surface for O_{3} molecule (ozone) was developed using high level *ab initio* electronic structure theory and the fitting by permutationally invariant polynomial functions. Another application of this fitting method was the construction of potential energy surface for molecular anion HCO^{–}.

15. SUBJECT TERMS

16. SECURITY CLASSIFICATION OF:			17. LIMITATION OF ABSTRACT	18. NUMBER OF PAGES	19a. NAME OF RESPONSIBLE PERSON
a. REPORT	b. ABSTRACT	c. THIS PAGE			19b. TELEPHONE NUMBER *(include area code)*

Non-Born-Oppenheimer Spectroscopy of Energetic Triatomics

This one-year project involved theoretical and computational studies of quantum dynamics and spectroscopy in the presence of conical intersection, when the Born-Oppenheimer approximation fails miserably due to a very significant geometric phase effect. We focused on cyclic-N_3 and studied spectroscopy of this radical in great detail, which included construction of its potential energy surface (PES) and the dipole moment function in the entire configuration space around the conical intersection, accurate calculations of its vibrational states using the state-of-the-art approach (gauge theory), detailed analysis of the geometric phase effect, calculation of transition intensities and, finally, prediction of its infrared spectrum. We were also able to construct new global potential energy surface for ozone molecule (O_3) using very high level of the *ab initio* electronic structure theory and fitting by permutationally invariant polynomial functions. Another product of this work was our contribution into construction of the potential energy surface for molecular negative ion HCO^-.

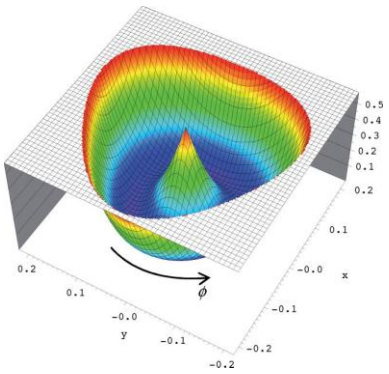

Fig. 1: Potential energy surface of cyclic-N_3 around the conical intersection.

The initial phase of this research began prior to the AFOSR grant, in order to generate preliminary data on cyclic-N_3. That preliminary work was very intense and resulted in the following four publications:

1. **D. Babikov**, P. Zhang, and K. Morokuma, "Cyclic-N_3: I. An accurate potential energy surface for the ground doublet electronic state up to the energy of the $^2A_2/^2B_1$ conical intersection", *J. Chem. Phys.* 121, 6743 (2004).
2. **D. Babikov**, B. Kendrick, P. Zhang, and K. Morokuma, "Cyclic-N_3: II. Large geometric phase effects in the vibrational spectra", *J. Chem. Phys.* 122, 44315 (2005).
3. V. A. Mozhayskiy, **D. Babikov** and A. I. Krylov, "Conical and glancing Jahn-Teller intersections in the cyclic trinitrogen cation", *J. Chem. Phys.* 124, 224309 (2006).
4. **D. Babikov**, V. A. Mozhayskiy and A. I. Krylov, "The photoelectron spectrum of elusive cyclic-N_3 and characterization of the potential energy surface and vibrational states of the ion", *J. Chem. Phys.* 125, 84306 (2006).

During the grant period we wrote four more papers:

5. **D. Babikov** and B. Kendrick, "The Infrared Spectrum of Cyclic-N_3: Theoretical Prediction", *J. Chem. Phys.* 133, 174310 (2010).
6. **D. Babikov**, "Perturbation theory treatment of pseudo-rotation in cyclic- N_3", *J. Chem. Phys*. 134, 114305 (2011).
7. M. Ayouz and **D. Babikov**, "Improved potential energy surface of ozone constructed using the fitting by permutationally invariant monomial functions", invited article to a *Special Issue in Advances in*

Physical Chemistry "Accurate potential energy surfaces and beyond: chemical reactivity, covalent bonding, long range interactions and spectroscopy", accepted.

8. M. Ayouz, I. Mikhaylov, **D. Babikov**, M. Raoult, S. Galtier, O. Dulieu and V. Kokoouline, "Potential energy and dipole moment surfaces of HCO^- for the search of H^- in the interstellar medium", *J. Chem. Phys.*, submitted.

We also have one manuscript in preparation. In what follows, we focus on three major achievements during the years 2010-2011, which cover the period of one-year grant plus the no-cost extension.

A. Construction of the global dipole-moment function of cyclic-N_3 and prediction of its infrared spectrum

The energies and wave functions of vibrational states of cyclic-N_3 were computed in adiabatically-adjusting principal-axis hyper-spherical coordinates (ρ,θ,φ), see Fig. 2, using and the sector-adiabatic coupled-channel technique. In this approach, the full dimensional Schrödinger equation for the vibrational motion is solved in two steps which can be thought of as numerical "decoupling" of different degrees of freedom. First, the hyper-radius ρ is partitioned into a large number of sectors and the two-dimensional eigenvalue problem is solved for θ and φ numerically for each sector with ρ fixed (as a parameter) at the center of the sector. In the second step, a set of one-dimensional coupled-channel equations is obtained for the hyper-radial coordinate ρ and is solved using a numerical propagation technique. In this procedure, the coupling is recovered and the accurate full dimensional solutions of the Schrödinger equation are obtained using the exact Hamiltonian and including all couplings.

Accurate *ab initio* potential energy surface from paper [1] was employed. The geometric phase effect was incorporated into our calculations using gauge theory. Further details about our method can be found in paper [2]. Figure 2 shows wave functions $\psi_i(\rho,\theta,\varphi)$ computed for progression of the pseudo-rotational states, labeled by the pseudo-rotational angular momentum quantum number, m, which takes half-integer values due to the geometric phase effect. There is

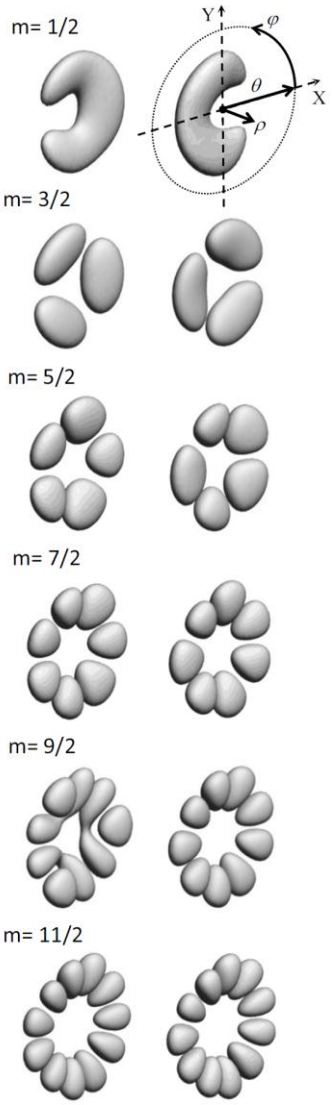

Fig. 2: 3D wave functions of cyclic-N_3 up to m = 11/2.

always a pair of states with the same value of m, one is symmetric (m^+) and another is anti-symmetric (m^-). States of *E*-symmetry are doubly-degenerate, while energies of *A*-symmetry states are spilt (A_1 and A_2). In Figs. 1 and 2 the conical intersection is located at origin $(x, y) = (0,0)$. The motion around it corresponds to pseudo-rotation and is described by the hyper angle φ. This coordinate is simply the polar angle covering the range of $-\pi < \varphi < \pi$. Wave functions presented in Fig. 2 indicate clearly that the vibrational motion around conical intersection in cyclic-N_3 is highly delocalized. Even the ground vibrational state (that corresponds, strictly speaking, to no vibrational excitation) allows encircling the conical intersection. Thus, for cyclic-N_3 the notion of equilibrium geometry does not carry any meaning.

One consequence of this floppiness is that the dipole moment function of cyclic-N_3 also has to be computed globally, everywhere around the conical intersection, not just at the vicinity of the minimum energy point of the PES. Moreover, since the dipole moment is a vector function, a careful transformation of its components should be carried out in order to describe rotation of the dipole moment vector in space, due to the pseudo-rotational nuclear motion. This is not straightforward and, to the best of our knowledge, has never been done in the past. Namely, two components of the dipole moment vector, μ_Q and μ_q, as produced for example, by MOLPRO package, are projections of the dipole moment vector $\boldsymbol{\mu}$ onto the principal axes of inertia of the molecule, **Q** and **q**. We have figured out the transformation of μ_Q and μ_q into the laboratory-frame components μ_x and μ_y, for an arbitrary molecular geometry (ρ, θ, φ). Details are given in paper [5], the final result is presented in Fig. 3 here: the 3D-functions for two components of the dipole moment vector, $\mu_x(\rho, \theta, \varphi)$ and $\mu_y(\rho, \theta, \varphi)$, allow computing rigorously all the matrix elements needed, namely:

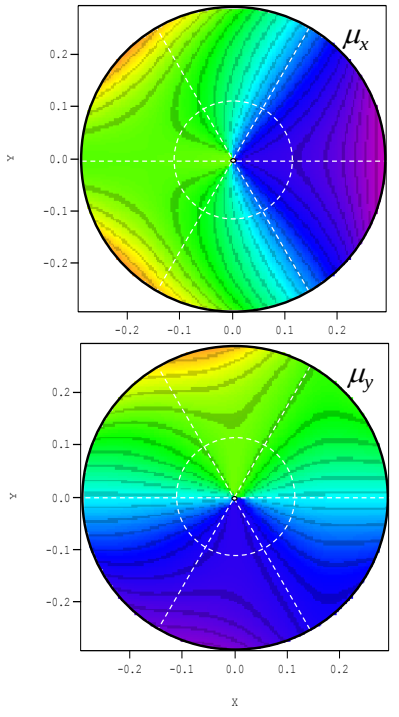

Fig. 3: Two components of the dipole moment vector function of cyclic-N_3

$$\mu_{ij}^{(x)} = \left\langle \psi_j(\rho,\theta,\varphi) \middle| \mu_x(\rho,\theta,\varphi) \middle| \psi_i(\rho,\theta,\varphi) \right\rangle,$$

$$\mu_{ij}^{(y)} = \left\langle \psi_j(\rho,\theta,\varphi) \middle| \mu_y(\rho,\theta,\varphi) \middle| \psi_i(\rho,\theta,\varphi) \right\rangle.$$

Analysis of the diagonal matrix elements has shown that the ground vibtational state of cyclic-N_3 exhibits the most significant permanent dipole moment. Four non-zero matrix elements for this doubly-degenerate state range from 77.3 to 96.3 mDebye. Note that the value of the dipole moment at the point of minimum on the potential energy surface is about 180 mDebye, while at the point of pseudo-rotational barrier it is about 160 mDebye (see Fig. 3). Thus, averaging over the vibrational wave function reduces the value of dipole moment roughly by a factor of two. Upper states of cyclic-N_3 possess smaller dipole moments, only about 10.0 mDebye for m = 3/2 states of *A*-symmetry, and only about 20.0 mDebye for m = 5/2 and 7/2 states of *E*-symmetry.

We found that the most important off-diagonal elements of the transition moment matrix in cyclic-N_3 correspond to excitation of the pseudo-rotational progression of states, when the transition is described by the following changes of quantum numbers: $\Delta v_1 = 0$, $\Delta v_2 = 0$, $\Delta m = +1$. The values of matrix elements for these transitions vary in the range between 58.5 and 108.0 mDebye. Transitions related to excitation of the bending and breathing modes exhibit much smaller transition moments. For comparison, some transitions characterized by the following changes of quantum numbers: $\Delta v_1 = 0$, $\Delta v_2 = +1$, $\Delta m = +1$, and $\Delta v_1 = +1$, $\Delta v_2 = 0$, $\Delta m = -1$, exhibit transition moments on the order of 0.1 mDebye. The most intense part of the predicted IR absorption spectrum is shown in Fig. 4. It includes seven purely pseudo-rotational excitation transitions with $\Delta m = +1$. First five of these transitions dominate the spectrum, with the values of absolute integrated absorption coefficients in the range between 0.5 and 1.2 km/mol. Frequencies of these five transitions are in the 75 to 275 cm^{-1} region, which is far infrared. We predict that the most intense is an m = 3/2 (A_1) → m = 5/2 (E) transition at 267.66 cm^{-1} (see Fig. 4). Two large splitting ($\Delta_{3/2}$ =100.46 cm^{-1}) and one small splitting ($\Delta_{9/2}$ = 2.45 cm^{-1}) should be observed in this part of spectrum due to transitions involving non-degenerate states of symmetries A_1 and A_2. We suggest using these features as accurate and very specific spectroscopic signatures of cyclic-N_3.

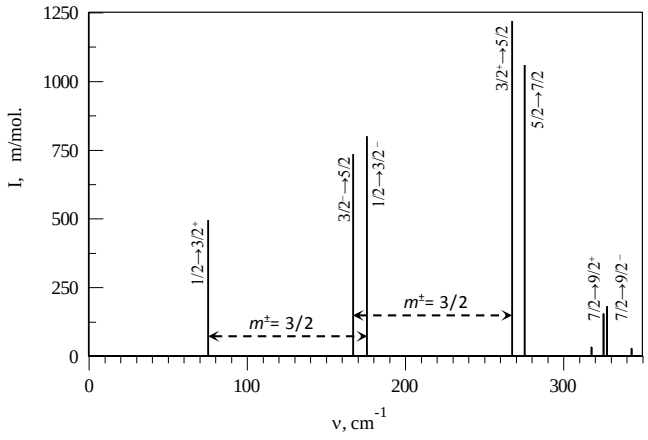

Fig. 4: The most intense far infrared part of the predicted absorption spectrum of cyclic-N_3.

B. Perturbation theory treatment of pseudo-rotational spectrum: towards analysis of the future experimental data

It is desirable to have a better intuitive understanding of the origin of splittings seen in the spectrum of Fig. 4 and to develop the means of relating the magnitudes of these splittings to major features of the potential energy surface of the molecule. This would be particularly useful for analysis of experimental spectrum of cyclic-N_3, where some transitions might be missing or technically inaccessible. With this purpose in mind we focused on qualitative and quantitative analysis of the lower pseudo-rotational states of cyclic-N_3 and developed a transparent theoretical treatment for them.

Figure 5 shows spectrum of lower pseudo-rotational states. Some of these states ($m = \frac{1}{2}, \frac{5}{2}, \frac{7}{2}$) are exactly degenerate pairs of *E*-symmetry, while others ($m = \frac{3}{2}, \frac{9}{2}$) are non-degenerate states of symmetries A_1 and A_2 with non-zero splittings. Values of these splittings are $\Delta_{3/2}$ =100.46 cm^{-1} and $\Delta_{9/2}$ = 2.45 cm^{-1}, for the states m = 3/2 and 9/2, respectively. In addition to these ten states our analysis incorporates some states calculated without inclusion of the geometric phase, namely: m = 0, 1, 2, 3 and 4. These states do not occur in nature (integer values of m) but they carry accurate information about the potential energy surface, important methodologically. For example, a pair of states with m = 3 (symmetries A_1 and A_2) show significant splitting, Δ_3 = –22.55 (see Fig. 5). The states with m = 1, 2, and 4 are exactly degenerate (symmetry *E*).

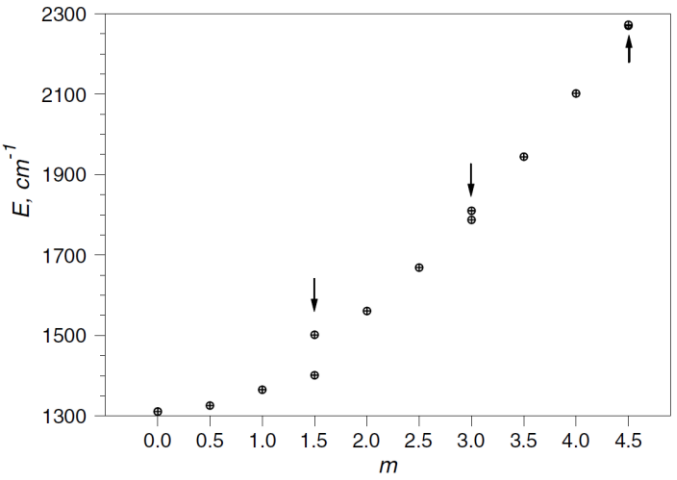

Fig. 5: Lower part of the pseudo-rotational spectrum of cyclic-N_3. Arrows indicate states of *A*-symmetry, where the splittings are observed.

We see that the value of splitting decreases as energy of states increases. In some cases the energy of symmetric state m^+ is below energy of the anti-symmetric state m^- (e.g., $m = \frac{3}{2}, \frac{9}{2}$) but there are cases when the order is reversed (e.g., $m = 3$). At lower energies the spectrum in Fig. 1 is near parabolic, typical to a rotor, but at higher energies (especially those outside of the range shown in Fig. 1) the spectrum flattens out towards a linear, typical to harmonic oscillator. *Can we explain all these*

features in a simple intuitive manner? Can we reproduce them accurately using a simple spectroscopy-like Hamiltonian?

We used analytical perturbation theory to solve this problem. Details are given in paper [6]. The major result is that the perturbation theory of second order can reproduce all features of this spectrum and fit it with the RMS deviation of only 0.26 cm^{-1}. The accurate spectrum computed numerically is shown in Fig. 5 by circles, while the analytic result of perturbation theory is shown by "+" symbols. On the scale of Fig. 5 these data are, basically, indistinguishable. The analytic expression obtained to fit the spectrum of pseudo-rotation states E_m is not particularly simple, but every parameter in it has very clear physical meaning:

$$E_m = E_m^{(0)} + E_m^{(1)} + E_m^{(2)} + E_m^{(3)},$$

$$E_m^{(0)} = ZPE + \frac{m^2}{2I_m},$$

$$E_m^{(1)} = \sum_n \frac{V_n}{2}\left[1 - \delta_{m,n/2} \cdot \frac{1}{2} s\right],$$

$$E_m^{(2)} = \sum_n \left(\frac{V_n}{2}\right)^2 \frac{I_m}{4n^2}\left(\delta_{m,n} \cdot 2s + \begin{cases} \dfrac{1}{(m/n)^2 - (1/2)^2}, & \text{if } m \neq n/2 \\ -1, & \text{if } m = n/2 \end{cases}\right),$$

$$E_m^{(3)} = -\sum_n \left(\frac{V_n}{2}\right)^3 \frac{{I_m}^2}{2n^4}\left(\delta_{m,n} \cdot 2s + \left[1 - \delta_{m,n/2} \cdot \frac{1}{2} s\right] \cdot \begin{cases} \dfrac{(m/n)^2 + (1/2)^2}{[(m/n)^2 - (1/2)^2]^2}, & \text{if } m \neq n/2 \\ 1/2, & \text{if } m = n/2 \end{cases}\right).$$

Here ZPE represents the zero-point energy of breathing and bending modes, I_m is the pseudo-rotational moment of inertia. In the simplest case it can be computed as $I_0 = \mu\rho_{\text{eq}}^2 \sin^2\theta_{\text{eq}} / 4$, where ρ_{eq} and θ_{eq} characterize equilibrium point of the potential energy surface, but using a simple second order dependence of I_m on the amount of pseudo-rotational excitation: $I_m = I_0 + I_1 m + I_2 m^2$, produces more accurate results. A set of coefficients $\{V_n\}$ represents expansion of the pseudo-

rotational PES near the bottom of the well: $V(\phi) = \sum_n V_n \cdot (1 - \cos n\phi)/2$. Since the potential energy surface is three-fold symmetric, only the terms with *n* = 3, 6, 9, *etc* are allowed. At the zeroth order of theory $V(\phi) = 0$. The first term with *n* = 3 creates three equivalent minima on the PES separated by three pseudo-rotation barriers, making the pseudo-rotation hindered at the first order of theory (the perturbation). The symmetry parameter is *s* = 1 for the m^+ states, while it is *s* = –1 for the m^- states; the standard Cronicker δ -symbol is used.

Major properties of this formula are as follows: Zeroth-order expression reproduces the overall trend of the spectrum but captures no splittings. The first-order correction shifts the entire spectrum (every *m*) by the same value of $\sum V_n / 2$, but also splits the pairs of degenerate zero-order states, each individually by the value of $V_{2m}/2$. Since only V_3, V_6, V_9, *etc* are present in the expansion of potential, the splitting occurs only for m = 3/2, 3, 9/2, *etc* states. Using the values of splittings and the expression $V_{2m} = 2\Delta_m$, one can obtain quick estimates for V_3 = 200.92 cm^{-1}, V_6 = –45.10 cm^{-1} and V_9 = 4.90 cm^{-1}. Note that the value of V_6 is negative, simply because the 3^- state lies below the 3^+ state. The second-order correction introduces the m -dependent shifts of individual states and affects only the splittings of states with integers values of m. Third order correction includes additional m -dependent shifts of all states, as well as splittings of all *A*-symmetry states with both integer and half-integer values of m.

TABLE II. The values of fitting parameters for analytical representation of the pseudorotational spectrum of cyclic-N_3 at various orders of the perturbation theory.

	Zeroth order	First order	Second order	Third order
ZPE, cm^{-1}	1306.05	1225.70	1228.06	1233.13
V_3, cm^{-1}	0.00	200.92	200.92	195.37
V_6, cm^{-1}	0.00	−45.10	−23.91	−29.23
V_9, cm^{-1}	0.00	4.90	4.90	4.90
I_0, cm	6.230×10^{-3}	6.230×10^{-3}	7.377×10^{-3}	6.815×10^{-3}
I_1, cm	9.807×10^{-4}	9.807×10^{-4}	6.178×10^{-4}	8.895×10^{-4}
I_2, cm	-7.102×10^{-6}	-7.101×10^{-6}	2.444×10^{-5}	-8.690×10^{-6}
χ^2, cm^{-2}	5539.03	235.67	0.88	52.23

The perturbation theory expression gives us seven parameters for a non-linear fitting problem: *ZPE*, I_0, I_1, I_2, V_3, V_6 and V_9. Table above summarizes their converged values for various orders of theory. First of all, we see that $I_0 >> I_1 >> I_2$ and $|V_3| >> |V_6| >> |V_9|$ conditions are fulfilled.

Contribution of the I_2 -term is very small, so that there is no reason to include the higher order terms. The second order correction affects significantly the value of V_6 (because it changes splitting of the *m* = 3 state) leaving the values of V_3 and V_9 unchanged and equal to those of the first-order theory. The values of V_3 and V_6 change when we go from the second to the third order, while the value of V_9 remains the same. We found that the value of V_9 is insensitive to the third order correction simply because effect of the third order (and probably of all higher orders) is negligible for this highly excited state. This feature is consistent with the general property of the perturbation theory – effect of the perturbation is higher for the lower energy states and becomes negligible at high energies. Thus we conclude that the value of V_9 is completely defined by the first-order theory, *i.e.*, directly by the splitting of the *m* = 9/2 states. The values of the χ^2 deviation characterize quality of the non-linear fit and we see that the second order of theory gives the best description. (The fact that the third order of perturbation theory gives result inferior to the second-order is well known. We did not attempt the fourth order of theory simply because the second order result is good enough.)

The quantitative success of the second-order expression demonstrated in this project suggests that the analytical perturbation theory expression can be confidently used for analysis of experimental data on cyclic-N_3. We wrote a FORTRAN code that can be used by experimentalists for analysis of the spectrum of cyclic-N_3.

C. Fitting the PES for a homonuclear triatomic molecule by the permutationally invariant polynomial functions

Potential energy surfaces of all homonuclear triatomics, like cyclic-N_3 or O_3, exhibit the three-fold symmetry (see Figs. 1 and 7). It is wise to utilize this symmetry in order to construct an efficient and accurate analytic representation of the PES. The fitting approach of Braams and Bowman allows building the symmetry into the functional form of the fit rigorously, taking full advantage of symmetry. We adopted this approach to construct PESs of homonuclear triatomic molecules, such as N_3 and O_3, and found that it allows obtaining accurate representation of complicate PESs with as few as 500-600 data points. If such small number of points is indeed sufficient, the electronic structure calculations can be carried out at a very high level of theory, which offers a very attractive method of building accurate PESs of N_3, O_3, and other highly symmetric homonuclear triatomic molecules.

Note that the fitting approach of Braams and Bowman does not require a structured grid. The data points can be anywhere on the PES. In this work we proposed a simple and general method for generating a small set of optimally placed points. Two reasonable criteria for choosing good points were (a) minimizing RMS of the global fit and (b) emphasizing most important parts of the PES (e.g., the minimum of the well, the transition state, or the conical intersection). Using the old surface of ozone, we pre-optimized a small set of 500 points to achieve the best description of the PES. Two following figures illustrate this procedure. Figure 6a shows initial positions of the 500 fitting points in the configuration space. In this example the initial placement of points was intentionally done in the worst possible way: All points sit very close to each other in one remote region of the PES. Coverage of the configuration space is minimal and the RMS deviation of the fit is huge, close to $5\times10^{12}\ \mathrm{cm}^{-1}$. We found that as points are moved, literally one by one, to their new better positions, the RMS deviation of the fit drops very quickly, roughly exponentially. After the first 200 points have been moved, the exponential fall regime transforms into an almost steady regime, where the RMS deviation of the fit fluctuates in the range between 33 and 50 cm^{-1}. Further iterations do not really improve the RMS deviation of the fit, but they promote the loss of "memory" of the initial placement of points. Figure 6b shows the final distribution of fitting points in the configuration space. It is not uniform. Some emphasis on the high energy part of the PES is clearly present, which means that this part of the PES is harder to fit accurately, compared to the well region at low energies. Some emphasis of the "reef" region is also seen.

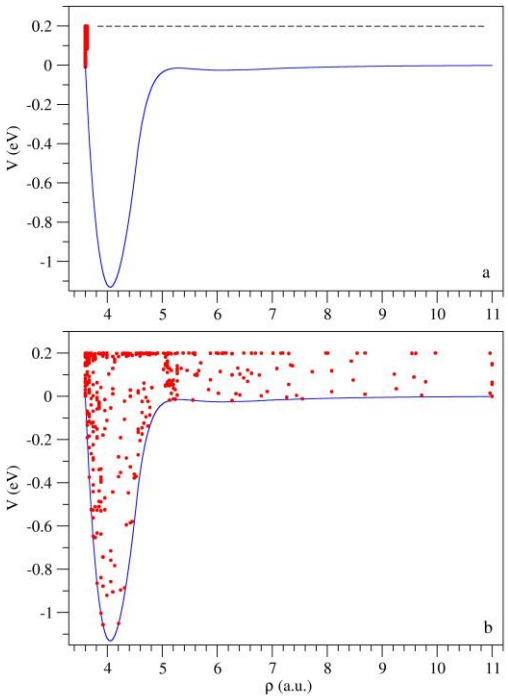

Fig. 6: Illustration of the pre-optimization procedure using the old surface of ozone. The MEP is shown as blue curve. The covalent well and the vdW well are seen. The 500 data points are shown as red dots.

The *ab initio* calculations were carried out using MOLPRO suite of the electronic structure codes. The level of theory was icMR-CISD+Q using the CASSCF(12,9) active space. At each point of the PES we did two independent calculations: first with aug-cc-pVQZ and second with aug-cc-pV5Z basis sets. Then, for each point of the PES, we made extrapolation to the CBS limit. The resultant value of the dissociation

energy at the CBS limit is $D_e = 1.135\,\text{eV}$, which is $871\,\text{cm}^{-1}$ higher than the dissociation energy of the old surface and only $65\,\text{cm}^{-1}$ lower compared to the recent experimental value. This represents a dramatic improvement.

The CBS data points were fitted by the permutationally invariant polynomial of 16th order as explained in paper [7]. The RMS deviation of the resultant fit was 26 cm^{-1} which is, in fact, slightly lower than the RMS deviation seen at the pre-optimization step. This result is quite encouraging and supports the idea (and efficiency) of pre-optimizing a set of data points prior to the massive *ab initio* calculations.

In Fig. 7 we show an iso-energy surface for the new PES of ozone in three dimensions. In this approach to PES visualization the configuration space where the potential energy of the molecule is higher than a given cut off value (here 0.2 eV above the dissociation threshold) is made transparent, while the configuration space classically accessible to the motion of nuclei at this energy is made visible as a 3D-structure. The hyper-spherical coordinates $\{\rho, \theta, \phi\}$ are used in order to emphasize symmetry of the PES. The range of hyper-radius in Fig. 7 is the same as in Fig. 6, namely 3.5 < ρ < 11 Bohr. Recall that the hyper-angles θ and ϕ correlate with bending and asymmetric stretching motions, respectively. Due to the permutation symmetry of ozone, there are three identical covalent wells in the entire configuration space, which can be reached by changing the value of ϕ. These are seen as three ellipsoidal-like lobes in the lower part of Fig. 7. They are connected to three energetically identical dissociation channels seen in the upper part of Fig. 7. The reef structures (the transition states) are seen on this picture as narrow bottlenecks connecting the covalent wells to the channels. Figure 7 gives global view of the PES and permits seeing all its features simultaneously. We also see that fitting by permutationally invariant polynomial function takes full advantage of symmetry of the molecule.

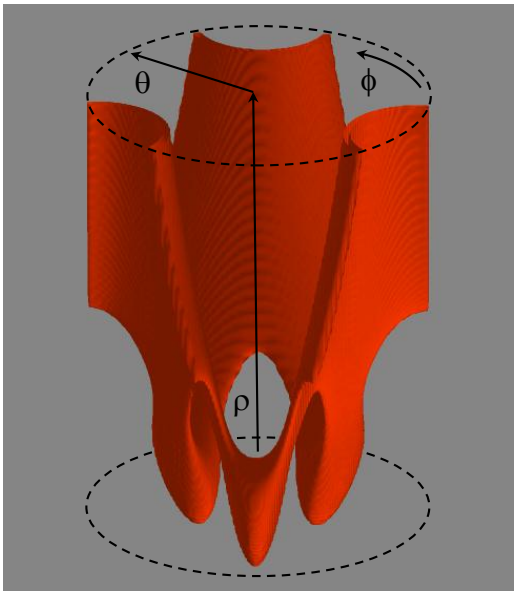

Fig. 7: Global view of the ozone PES in three dimensions using iso-energy surface at 0.2 eV and the internal hyper-spherical coordinates.

The same fitting approach was used to build the PES of HCO^-. Details were reported in paper [8].